Math.Comput.Sci. (2022) 16:8
https://doi.org/10.1007/s11786-022-00521-y

Mathematics in Computer Science

Load Bearing Capacity of Light Timber Frame Walls Under Fire

Paulo A. G. Piloto · **Elza M. M. Fonseca**

Received: 3 May 2021 / Revised: 14 December 2021 / Accepted: 15 February 2022

Abstract Light Timer Frame Walls are made of solid timber elements and are usually fire protected by other materials. This investigation determines the residual load bearing capacity of Light Timber Frame Walls for fire rating periods of 30, 60, 90 and 120 min. The timber frame is made with 3 studs and 2 tracks, using two different fire protection levels (one and two gypsum layers). The computational model includes the thermal analysis under standard fire, including all types of materials and a sequential mechanical analysis with incremental load applied for each fire rating periods, applied just for the load bearing material. Nonlinear solution methods are used with small tolerance values for solution convergence, to determine the correct temperature and displacement fields. The thermal and the mechanical properties are considered temperature dependent. The mechanical analysis considers large displacement behaviour, and the charring effect of wood is included by the reduction of the stiffness and strength of the timber. The results show that the load bearing capacity decreases with the fire exposure time. A new proposal is presented between the load bearing capacity and the fire rating and finally the char layer is compared with the current and future version of Eurocode 5, part 1.2.

Keywords Fire · LTFW walls · Load bearing · Charring rate · Finite element method

1 Introduction

Light Timber Framed Walls (LTFW) are made with solid wood members (studs and tracks) used on buildings, for load bearing and partition walls. The assemblies are made with solid stud wood vertical members, usually separated by 400–600 mm. The cladding for internal walls may be developed by wood panels, composite panels and or gypsum panels. The number of protection layers and insulation materials used in the cavities of the wall depends on the thermal and acoustic efficiency required to the LTFW at room temperature, but also depends on the fire rating of LTFW required.

Paulo A. G. Piloto (✉)
Instituto Politécnico de Bragança, Campus de Santa Apolónia, 5300-253 Bragança, Portugal
e-mail: ppiloto@ipb.pt

Elza M. M. Fonseca
Mechanical Engineering Department, School of Engineering, Polytechnic Institute of Porto, Rua Dr. António Bernardino de Almeida, 431, 4249-015 Porto, Portugal
e-mail: elz@isep.ipp.pt

Published online: 07 April 2022

Birkhäuser

Wood has been widely used in building due to its good environmental impact. However, timber structures are highly vulnerable to fire because of their combustion process. Due to its own composition, wood is a combustible material. Nevertheless, wood burns slowly and is not easy to ignite if there is no spark or flame nearby. Initially, when submitted to fire conditions, wood temperature starts to rise, losses free water by evaporation and starts drying. Near 100 (°C), temperature keeps constant for a short period and then starts to rise with the release of pyrolysis gases. Wood oxides and becomes dark. When approaching 300 (°C), variable according to species, ignition takes place and an exothermal, reaction takes place. Without the presence of direct flame or spark, wood requires a higher temperature to be ignited. After this process, burning is developed in the pyrolysis region, consuming intact wood, producing the charring layer. To avoid premature failure of timber frame structures, protection layers or cladding is applied to make the assembly fire resistant.

For the case of load bearing walls, the vertical load is transmitted through the studs and panels may increase the stability of the vertical elements, depending on the stiffness of the connection between the panels and the studs. Panels may be also supporting orthogonal and in plane loads, in the case of external walls submitted to wind loads and seismic loads. The fire resistance should be verified for the load bearing capacity (R), insulation (I) and integrity (E), usually using experimental standard tests, specimen instrumentation and criteria defined on EN1363-1 [1], EN1365-1 [2], ISO834 [3]. The load bearing (R) establishes the ability to withstand the test load and the criterion is defined based on the vertical contraction displacement or rate of displacement. The integrity (E) establishes the ability to withstand the flames and hot gases coming from the exposed side of the wall and the criterion is defined based on the detection of the ignition of a cotton pad or any growing cracks or opening in the unexposed side. The criterion (I) establishes the ability to reduce the heat flow from the exposed side to the unexposed side, avoiding the ignition of any combustible material. The criterion is based on the measurement of the unexposed temperature [1].

For the case of non-load bearing walls, the fire resistance should be verified for the insulation (I) and integrity (E), usually using the same type of procedures EN1363-1 [1], EN1364-1 [4], ISO834 [3].

Load bearing and partition wall systems used in residential and commercial properties are required to provide fire rating according to times established in the fire classification of construction products and building elements, EN13501-2 [5]. Partition walls can be rated for EI = 15, 20, 30, 45, 60, 90, 120, 180 and 240 (min), while the load bearing elements can be rated for $REI = 15, 20, 30, 45, 60, 90, 120, 180, 240$ and 360 (min). The safety level is then selected by each European country, using its own national regulation system.

During the last years, only a few experimental tests have been carried out. Takeda and Mehaffey [6] developed some experimental tests, that authors have already validated, using 2D numerical models using Ansys [7]. Thomas [8] tested the suitability of the finite element heat transfer program SAFIR [9] for modelling plasterboard-lined LTF assemblies. Similar results were obtained with the program TASEF [10] with slight differences. Both programs seem to give better overall results for slower developing fires and furnace tests than more rapidly growing fires. This research also concludes that more sophisticated models, including mass transfer, effect of connections, gaps between panels and ablation are required to achieve better comparisons. Thi et al. [11] studied the behaviour of cross-laminated timber (CLT) panel in the central part of the wall system, where the pyrolysis of timber was modelled explicitly in the energy equation, implementing a user subroutine called UMATHT, in Abaqus for thermal analysis. The falling off the gypsum boards under fire was considered implicitly in the FE model based on experimental observations. Results show the need to consider explicitly the cracks and falling off the gypsum boards for an appropriate prediction of the integrity fire resistance. Bedon and Fragiacomo [12] developed an experimental and finite element study to evaluate the fire behaviour of unprotected log-haus timber walls in fire conditions under in-plane compressive loads. Numerical results were validated, and a parametric analysis was performed, considering the most important parameters. The effects of these parameters were presented in terms of overall buckling resistance and failure modes, providing evidence for the reduction the load bearing capacity. Fonseca et al. [13] determined the fire resistance of unprotected wood connections and evaluated the efficiency of the protection using different types of gypsum plasterboard. Qin et al. [14] made experimental tests to evaluate the fire behaviour of wood components under different service loads. The authors concluded that service load can accelerate the charring rate and increase the charring depth, proposing a new formula to determine the charring rate, depending on the service load.

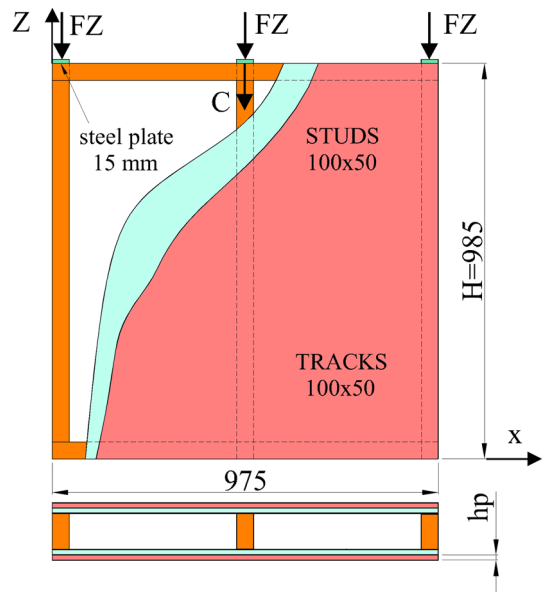

Fig. 1 Light timber frame wall assembly

Table 1 Specimens used for the numerical simulation of LTFW

Specimen	Protection layers gypsum	Fire scenario exposed surface	Fire scenario inside cavity
01	1 × hp = 12.5 (mm)	ISO 834 [3]	FIRE CAVITY 01 [15] (Specimen 08)
02	2 × hp = 12.5 (mm)	ISO 834 [3]	FIRE CAVITY 02 [16] (Specimen 11)

This numerical investigation deals with two different levels of fire protection applied to LTFW, evaluating the load bearing capacity for different fire rated times. The simulations are based on a two-step simulation process, submitting the LTFW under the thermal effect of the fire, using two experimental fire scenarios used for LSF (Light Steel Frame) walls developed by Piloto et al. [15] and Khetata et al. [16] (single layer protection during 60 min and double layer protection during 120 min) and then for each fire rated time a thermomechanical analysis is developed to determine the load bearing capacity. For the first fire scenario, the load bearing capacity is determined for R30 and R60, while for the second fire scenario, the load bearing capacity may be determined for R30, R60, R90 and R120. In both cases, the position of the char line is determined in timber members, assuming the position of the 300 (°C) isothermal, making the comparison with the Eurocode 5, part 1.2, current version [17] and the future version [18].

2 Materials and Methods

The LTFW assemblies under evaluation are made with softwood Douglas fir, using 3 solid timber elements for studs and 2 solid timber elements for tracks, each with a cross section of 100x50 (mm). The dimensions are defined according to the furnace dimensions, see Fig. 1.

The specimens are simulated according to the conditions presented in Table 1. The fire scenario inside the cavity includes the effect of the falling off and damage of gypsum plates during experimental tests. This damage effect has been considered by an additional boundary condition inside the cavity, considering the measured cavity temperature as the bulk temperature required for heat transfer by radiation and convection in this region.

The fire scenarios are depicted in Fig. 2 and two different fire durations are considered. The fire cavity 01 is typically used for 1 h of standard fire, being the temperature in the cavity region defined by this curve. The fire cavity 02 considers a standard fire event of 2 h and the temperature in the cavity is also depicted. Both curves are

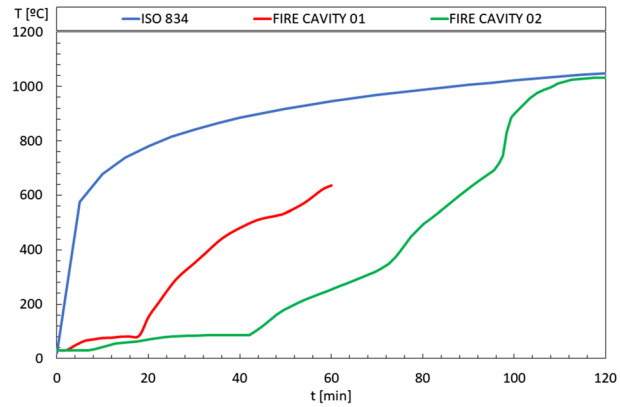

Fig. 2 Fire curves used for the simulation of light timber frame walls

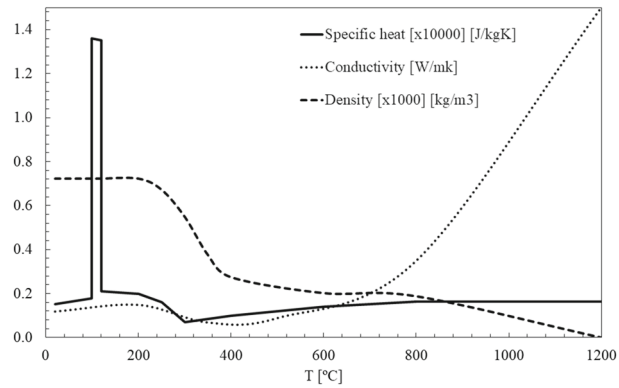

Fig. 3 Thermal properties for wood

compared with the same standard fire used for the exposed surface. The main difference between fire cavity 01 and 02 is related to the insulation level of the cavity region. The cavity of specimen 01 will be exposed to fire after 19 (min), while the cavity of specimen 02 is going to be exposed after 41 (min).

2.1 Material Properties

The material properties involved in these simulations are the thermal properties for wood and gypsum (conductivity, specific heat density and emissivity) and the mechanical properties for wood members (elastic, plastic, and damage criterion). Gypsum is not considered for load bearing even with the existence of self-screwing bolts.

The thermal properties for both materials involved in the thermal simulation are presented in Figs. 3 and 4. They are based on the EN1995-1-2 [17] and based on Sultan investigation [19]. The emissivity of both materials is equal to 0.8.

The mechanical properties are only presented for the material that is capable to bear the vertical load. Wood is a highly anisotropic material, due to the way a tree grows and the arrangement of the wood cells within the stem. Wood can be considered locally as an orthotropic material that possesses three principal directions. The softwood model considers different behaviour of the material in the direction of the fibres, radial direction, and tangential direction. The strength and stiffness of wood are considerably higher in the longitudinal than in the orthogonal directions. This can be easily understood on the basis of $90 \pm 95\%$ of the fibres are longitudinally oriented [20]. The generalized Hooke law for an orthotropic material is considered. Table 2 gives the temperature dependent properties used for the elastic behaviour of the material.

Moreover, According to EN1995-1-2 [17] it is possible to conclude that the strength for wood in the direction parallel to the grain is linearly reduced with increasing temperature, more accentuated up to 100 (°C). The modulus

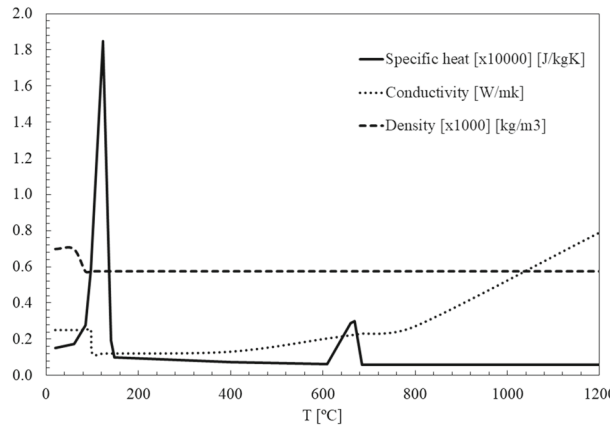

Fig. 4 Thermal properties for gypsum

Table 2 Linear elastic orthotropic properties for softwood Douglas fir [17,21]

	20 (°C)	100 (°C)	300 (°C)
E_X (Pa)	11.20×10^9	5.600×10^9	0.112×10^9
E_Y (Pa)	0.448×10^9	0.224×10^9	0.004×10^9
E_Z (Pa)	0.985×10^9	0.493×10^9	0.009×10^9
ν_{XY}	0.315	0.315	0.315
ν_{YZ}	0.308	0.308	0.308
ν_{XZ}	0.347	0.347	0.347
G_{XY} (Pa)	0.907×10^9	0.454×10^9	0.009×10^9
G_{YZ} (Pa)	0.123×10^9	0.061×10^9	0.001×10^9
G_{XZ} (Pa)	1.075×10^9	0.538×10^9	0.010×10^9

of elasticity is also affected by the increase in temperature. The reduction factors were used for 100 and 300 (°C). Poisson's coefficients are considered constant in the face of temperature rise, because the current version [17] and future version [18] of the EN1995-1-2 do not define correction factors to be applied for this property. The transverse elastic modulus also undergoes a reduction with increasing temperature, and the same reduction coefficients of the modulus of elasticity are used, since both elastic properties of wood are related through Poisson's coefficients.

The rupture of wood can be presented itself in several ways, such as fibre breakage, micro-cracking of the matrix, detachment of fibres or delamination. To characterize this effect, the Hill criterion is adopted [22]. Hill's criterion [23] considers the interaction between the stress in the failure mechanism and depends on the orientation of the stress in relation to the anisotropy axis of the material. This criterion allows the determination of the elastic and elastoplastic zones in the stress-strain relationship of the wood. adopted to simulate orthotropic plastic behaviour. The Hill stress potentials are dependent only upon the deviatoric stress, so that the plastic part of the response is incompressible. Hill's stress potentials, in terms of rectangular cartesian stress components σ_{ij} are given by Eq. (1), where constants F_{ii} and N_{ij} are functions of the ratio of the scalar yield stress parameter and the yield stress in each of the six stress components.

$$f^y\left(\sigma_{ij}\right) = \sqrt{\begin{bmatrix} F_{11}\left(\sigma_{22}-\sigma_{33}\right)^2 + F_{22}\left(\sigma_{33}-\sigma_{11}\right)^2 + F_{11}\left(\sigma_{11}-\sigma_{22}\right)^2 + 2N_{12}\sigma_{12}^2 \\ +2N_{23}\sigma_{23}^2 + 2N_{13}\sigma_{13}^2 \end{bmatrix}} \tag{1}$$

The characteristic parameters of the anisotropy of the material, determined for the criterion are the R_{ij} yield rates, established as a function of the limit stress in the main directions of the material, where the directional yield stress ratios are the user-input parameters and are related to the isotropic yield stress parameter. knowing that the wood does not have the plastic capacity and knowing that the perfectly elastic-plastic regime is considered in the

Table 3 Strength limit in tension and Hill criterion coefficients for softwood Douglas fir [17,21]

	20 (°C)	100 (°C)	300 (°C)
f^y (Pa)	44.90×10^6	28.92×10^6	0.449×10^6
$R_{XX} = f^y_{xx}/f^y$	1	1	1
$R_{YY} = f^y_{yy}/f^y$	0.052	0.052	0.052
$R_{ZZ} = f^y_{zz}/f^y$	0.052	0.052	0.052
$R_{XY} = f^y_{xy}\left(f^y/\sqrt{3}\right)$	0.405	0.405	0.179
$R_{YZ} = f^y_{yz}\left(f^y/\sqrt{3}\right)$	0.405	0.405	0.179
$R_{XZ} = f^y_{xz}\left(f^y/\sqrt{3}\right)$	0.405	0.405	0.179

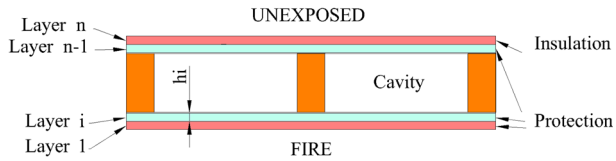

Fig. 5 Timber frame wall lined with gypsum plates, with basic layers for protection and insulation

model of this study just to ensure that the material has an elastic limit. The tensile strength f^y_{xx} are temperature dependent, being the values equal to 44.49, 28.92 and 0.44 (MPa), for 20, 100 and 300 °C, respectively [17]. Table 3 gives the yielding rates used for each orthogonal direction and temperature level.

2.2 The Separating Function Method

The separating function method is based on the component additive method, firstly developed in 2009 by Schleifer [24]. The total fire resistance for insulation is determined by the sum of the protection layers considering different heat transfer paths, see Fig. 5.

In 2010, based on experimental tests and numerical simulations for the heat transfer through separating multiple layered construction elements, Frangi et al. [25] also presented the simplified model for the verification of LTF wall structures. This method is already included in the new generation of the EN 1995-1-2 [18] and significantly improves the design method in the current version of EN 1995-1-2 [17]. This method is based on a component additive model, in which the fire resistance is obtained from the sum of resistance values obtained in each layer (protection, cavity, and insulation). The method has been well presented for light timber frame walls by Mäger et al. [26] and by Mäger et al. [27]. The separating function method assumes that, with minimal requirements on detailing, integrity is satisfied when the insulation criterion is satisfied. The coefficients of the design method (basic values, correction time and position coefficients) are only applied to non-load bearing LTF walls, but they are presented to be compared with the non-linear thermal analysis.

The total fire resistance is therefore taken as the sum of the protection time defined by each protection layer and the insulation time given by the last layer "*n*". The improved design method is based on the summation effect of each layer (cladding and cavity) and gives the fire resistance due to the insulation ability of the assembly. The total insulation time is based on the most critical heat flow pattern (any position between wood studs), and is calculated by Eq. (2).

$$t_{\text{ins}} = \sum_{i=1}^{n-1} t_{\text{prot},i} + t_{\text{ins},n} \tag{2}$$

The first summation gives the protection time $t_{\text{prot},i}$ (min) of the layers preceding the last layer of the assembly, see Fig. 5. The insulation time due to the last layer is given in (min) by $t_{\text{ins},n}$. The total insulation time is t_{ins}

Table 4 Basic values for protection layers and insulation layer [25], h_i (mm)

Material	Basic insulation $t_{ins,0,n}$ (min)	Basic protection $t_{prot,0,i}$ (min)
Gypsum	$24 \times (h_i/15)^{1.4}$	$30 \times (h_i/15)^{1.2}$

Table 5 Position coefficients affecting the exposed protection layers and exposed insulation layer [7]

Material	$k_{\text{pos,exp},n}$ for insulation	$k_{\text{pos,exp},i}$ for protection
Cladding (gypsum, timber)	$1 - 0.6 \times \frac{\sum t_{prot,n-1}}{t_{ins,0,n}}$, if $\sum t_{prot,n-1} \le \frac{t_{ins,0,n}}{2}$ $0.5 \times \sqrt{\frac{t_{ins,0,n}}{\sum t_{prot,n-1}}}$, if $\sum t_{prot,n-1} > \frac{t_{ins,0,n}}{2}$	$1 - 0.6 \times \frac{\sum t_{prot,i-1}}{t_{prot,0,i}}$, if $\sum t_{prot,i-1} \le \frac{t_{prot,0,i}}{2}$ $0.5 \times \sqrt{\frac{t_{prot,0,i}}{\sum t_{prot,i-1}}}$, if $\sum t_{prot,i-1} > \frac{t_{prot,0,i}}{2}$

Table 6 Position coefficients affecting the unexposed side of the protection layers [25], h_i (mm)

Material	$k_{\text{pos,unexp},i}$ for layers backed by cladding made of gypsum and timber	$k_{\text{pos,unexp},i}$ for layers backed by insulation material in the cavity
Cladding (Gypsum)	1.0	$0.5 \times (h_i)^{0.15}$

The protection time for the layers preceding the last one should be calculated using their basic values, the coefficients for their positions, the coefficients for the joints and the correction times, according to Eq. (3).

$$t_{\text{prot},i} = (t_{\text{prot},0,i} \times k_{\text{pos,exp},i} \times k_{\text{pos,unexp},i} + \Delta t_i) \times k_{j,i} \tag{3}$$

The protection time for the last layer should be given by Eq. (4), considering the basic insulation time, the coefficient for its position, the correction time and the coefficient for the joints.

$$t_{\text{ins},n} = (t_{\text{ins},0,n} \times k_{\text{pos,exp},n} + \Delta t_n) \times k_{j,n} \tag{4}$$

For all the proposed factors, the next tables should be applied. The basic values correspond to the fire resistance of a single layer without the influence of adjacent materials, see Table 4.

The position coefficient for layer "i" may be defined as the ratio between the contribution to the fire resistance of the layer $t_{\text{prot},i}$, concerning its basic protection $t_{\text{prot},0,i}$. The influence of the layers preceding and backing the layer under analysis "i" is included by the coefficient $k_{\text{pos,exp},i}$ and $k_{\text{pos,unexp},i}$.

The contribution to the fire resistance of the layer "$i + 1$" is usually smaller than the contribution of the layer "i" because previous protection layers are falling off exposing the current protection layer to a higher temperature level, which means that is submitted to a different boundary condition when compared to the previous one.

The position coefficients were presented by Frangi et al. [25], assuming that the layers fell off when the temperature on the unexposed side of each layer protecting layer increased by 250 °C above the initial average temperature, see Tables 5 and 6. This assumption is assumed by the same authors as conservative.

Based on the experimental results and numerical simulations, Frangi et al. [7], showed that the influence of the layer backing the layer under consideration "i" is small, if the backing layer is made of gypsum or wood, which explains the value 1.0, see Table 6. The influence of the insulation material, backing the layer under consideration "i" is important, because the temperature of that layer increases faster.

The effect of the cavity without insulation material is considered by a modification of the coefficients for position of each layer in contact with the cavity, see Table 7.

The correction times are presented in Table 8, to compensate for the assumed conservative approach. These correction times were calculated by finite element simulations, using a temperature criterion of 600 °C for the boards falling off, see Table 8. These correction times should only be used in case of layers protected (preceded) by type F gypsum plasterboards and gypsum fibre boards. These correction times are being modified in the current proposal for the next generation of the EN1995-1-2 [18].

Table 7 Modified position coefficients affecting the protection layers and insulation layer due to the existence of a void cavity [7]

Material	Layer on the exposed side	Layer on the unexposed side
Cladding (Gypsum, timber)	$k_{\text{pos,unexp},i}$ see Table 6, column 3	$1.6 \times k_{\text{pos,exp},i}$ see Table 5 $3 \times \Delta t_i$ or $3 \times \Delta t_n$ see Table 8

Table 8 Correction times used for protection and insulation [25]

Material	Δt_n for $t_{ins,n}$ (min)	Δt_i for $t_{prot,i}$ (min)
Cladding (Gypsum, timber)	$0.03 \times t_{prot,n-1} + 0.9 \times t_{ins,0,n} - 2.3$, $t_{ins,0,n} < 12\,min$ $0.22 \times t_{prot,n-1} - 0.1 \times t_{ins,0,n} + 4.7$, $t_{ins,0,n} \geq 12\,min$	$0.03 \times t_{prot,i-1} + 0.9 \times t_{prot,0,n} - 2.3$, $t_{prot,0,i} < 12\,min$ $0.22 \times t_{prot,i-1} - 0.1 \times t_{prot,0,i} + 4.7$, $t_{prot,0,i} \geq 12\,min$

The coefficients that accounts for the effect of the joints are not included in this investigation, because all the simulations were assumed without joints. The existence of joints is allowed up to the limiting value of 2 mm, according to the next generation of EN1995-1-2 [18]. For simplicity, this design method considers the influence of joints in the insulation layer and for the layer preceding a void cavity. For all the other layers, the unit value should be considered.

2.3 The Charring of Members in Wall Assemblies

The char layer can provide some level of protection to the heat flux received by the fire event. The existence of the gypsum layers (cladding) with respect to the timber frame, delays the start of the charring. The time to start charring is herein considered by t_{ch}. The failure time of the cladding is defined by t_f, while the specific time to achieve a charring depth of 25 mm is t_a . There is an increase in the charring rate immediately after the falling off of the gypsum layers, since the bulk temperature is much higher and the effective protection of the char layer is only achieved after reaching 25 mm. When the char layer achieves this value, the charring rate decreases.

According to the current version of EN1995-1-2 [17], and for claddings consisting of one layer of gypsum, the time to start charring t_{ch} is 21 min, and should be calculated according to Eq. (5), where h_p is the thickness of the gypsum layer in millimetre.

$$t_{ch} = 2.8 \times h_p - 14 \tag{5}$$

For claddings consisting of two layers of gypsum plasterboard of type F, the start of charring t_{ch} should be determined according to Eq. (4) where the thickness h_p is taken as the thickness of the outer layer plus 80% of the thickness of the inner layer, providing that the spacing of fasteners in the inner layer is not greater than the spacing of fasteners in the outer layer, in this case, 49 min.

The time limit t_a, depends on the notional design charring rate β_n and depends on the time to fail the protection, which is herein considered equal to t_{ch} see Eq. (6). The k_3 factor should be considered equl to 2. For any time higher than t_a the charring rate should be applied without the multiplication by the factor k_3.

$$t_a = \frac{25}{k_3 \beta_n} + t_f \tag{6}$$

The notional design charring depth $d_{char,n}$ is calculated according to Eq. (7).

$$d_{char,n} = \sum_{Phases} \beta_n \times t \tag{7}$$

According to the next generation of EN1995-1-2 [18], there are some modifications to be considered. The European charring model is applied only to standard fire exposure ISO834. Several phases should be taken into

account, when relevant. The first phase is defined when no charring occurs behind the fire protection system t_{ch} . The second phase is defined when charring occurs behind fire protection system, while the protection layers is still in place $t_{f,pr}$. This time event has been considered coincident with t_{ch}. The third phase is defined after the failure of the fire protection layer and runs up to the development of 25 mm charring thickness t_{ch}. After this event, the new phase reduces the charring rate, as expected.

The notional design charring depth should be calculated as previously defined in Eq. (7). The time for starting the charring has been considered equal to the time to failure of the gypsum layer $t_{f,pr}$. For the case of a single layer, one can use Eq. (8), while for the case of two layers one should be using Eq. (9), where h_p considers the thickness of multiple layers of the same material.

$$t_{ch} = t_{f,pr} = 4.6 \times h_p - 25 \tag{8}$$

$$t_{ch} = t_{f,pr} = 4.4 \times h_p - 50 \tag{9}$$

The consolidation time should be calculated according to Eq. (10).

$$t_a = min \begin{cases} 2 \times t_{f,pr} \\ t_{f,pr} + \frac{25-(t_{f,pr}-t_{ch})\times\beta_{n,Phase2}}{\beta_{n,Phase3}} \end{cases} \tag{10}$$

The notional charring rates of the timber member should be determined according to Eqs. (11) and (12) for the third and fourth phases, respectively. The basic design charring rate was considered equal to 0.65 mm/min, when considering the timber frame made of softwood.

$$\beta_n = k_{3,1} \times k_{s,n,1} \times \beta_0 \tag{11}$$

$$\beta_n = k_{s,n,2} \times \beta_0 \tag{12}$$

The simplified relationship of charring phases is defined in the next section, presenting the comparison with the numerical results.

2.4 Finite Element Model for Thermal Analysis

The finite element model considers different types of elements for thermal and mechanical analyses, using ANSYS software. Both analyses are decoupled. Mechanical deformations do not produce any temperature change, but the opposite is true, that is, the change in temperature affects the mechanical properties and consequently the equilibrium of the timber structure. For this reason, thermal analysis must be performed before the mechanical analysis. For the thermal analysis, only the hexahedron SOLID70 is used. This element has eight nodes, each with one degree of freedom (temperature), uses linear interpolating functions and full Gauss integration 2 × 2 × 2. The mesh is defined in Fig. 6, after a convergence test of the solution, for both specimens. The number of elements was obtained through a convergence test. The solution method is considered incremental and iterative, due to the non-linearities involved in the materials properties and boundary conditions. The time step was selected to be 60 (s), but can be reduced to 1 (s). The criterion used for convergence is based on the heat flow, using a tolerance value of 1% and a reference value of 10^{-6}.

The heat conduction inside the physical domain, corresponding to the LTFW, is mathematically modelled by the energy conservation equation, see Eq. 13, where T represents the temperature (°C), ρ(T) is the specific mass (kg/m^3), Cp(T) is the specific heat (J/kgK), λ(T) is the thermal conductivity (W/mK), t is the time (s) and $\nabla = (\partial x, \partial y, \partial z)$ is the gradient. Equation (13), is based on the heat flow balance, for the infinitesimal material volume, in each spatial direction.

$$\rho\,(T)\,C_p\,(T)\,\frac{\partial T}{\partial t} = \nabla\cdot(\lambda\,(T)\,\nabla T) \tag{13}$$

Equation 13 is time-dependent because the heat flux on the boundary exposed to the fire change with time, i.e, the thermal state of the LTFW is transient. The incremental and iterative solution of Eq. (13) is required to determine

the temperature inside the physical domain along the time and, consequently, determine the fire resistance, besides the position of the 300 [a]C isothermal to define the moving of the pyrolysis process expected in wood. The boundary conditions applied in this model follows the requirements of the EN1991-1-2 [28]. This document establishes that for the exposed side of the LTFW, the convection coefficient $\alpha_c = 25$ (W/m^2 K) should be used for ISO 834 standard fire exposure, see Eq. (14), whilst for the unexposed side the total heat transfer coefficient, α_c, equals 9.0 (W/m^2 K) when assuming the effects of combined radiation and convection, see Eq. (15). Additionally, the emissivity of the flames is considered $\varepsilon_f = 1.0$. The initial temperature of the LTFW is constant and equal to $T_0 = 20$ (° C) applied to all nodes of the model. An extra boundary condition is applied in the cavity region, determined by experimental observations, that will help the model to consider the damaging effect of the gypsum material. The bulk temperature is defined by the fire scenario expected for the cavity, see Table 1. The radiation boundary condition is also included in the cavity region.

$$\lambda\,(T)\,\nabla T\vec{n} = \alpha_c\,(T_\infty - T) + \phi\epsilon_m\epsilon_f\sigma\left(T_\infty^4 - T^4\right) \tag{14}$$

$$\lambda\,(T)\,\nabla T.\vec{n} = \alpha_c\,(T - T_{\infty=20}) \tag{15}$$

where $\vec{n}$ the unitary vector normal to the external face, ϕ is the view factor, α_c is the convection coefficient, ε_m is the emissivity of the material, σ the Stefan–Boltzmann constant and T_∞ the gas temperature of the fire compartment according to standard ISO834 [3], while the bulk temperature in the unexposed side $T_{\infty=20}$ is considered equal to 20 °C , see Fig. 5. Eq. (14) is based on the heat flow that enters to the exposed surface of the LTFW (by conduction) and that arrives by heat transfer (radiation and convection), using the gas bulk temperature.

Based on previous numerical research [16], the extra boundary condition is applied to all the internal surfaces of the cavity. The convection coefficient is set to be $\alpha_c = 17$ (W/m^2 K) and the emissivity of the flames is $\varepsilon_f = 1.0$, assuming that the bulk temperature of the cavity is following the fire cavity curves defined in Fig. 2. The convection coefficient is an average value between the exposed and unexposed side. This value may be justified by the fact that the cavity is not directly exposed to fire during all fire test, depending on the gypsum cracking and falling off.

The general procedure of the finite element method for solving Eq. 13, is based on the weak-form Galerkin model [29] and from the minimum condition for the weighted residual method, leading to the matrix format of the energy equation, see Eq. 16, where the matrix $C_{(T^{n+1})}$ is the capacitance matrix, $T^{n\cdot}$ is the nodal vector for temperature at the time instant t_n, $K_{(T^{n+1})}$ the conductivity matrix and $F_{(T^{n+1})}$ the vector of the thermal loads.

$$C_{(T^{n+1})}\frac{T^{n+1} - T^n}{\Delta t} + \theta K_{(T^{n+1})}T^{n+1} = F_{(T^{n+1})} - (1-\theta)\,K_{(T^{n+1})}T^n \tag{16}$$

The built-in ANSYS solution method for Eq. 16 is based on the approximation of the time derivative by forward finite difference $\dot{T} \approx (T^{n+1} - T^n)/\Delta t$, where $\Delta t = t_{n+1} - t_n$, jointly with $T \approx (1-\theta)\,T^n + \theta\,T^{n+1}$, being $0 < \theta < 1$. The solution method uses Newton–Raphson method at each time step.

The finite element mesh is depicted in Fig. 6, for both specimens.

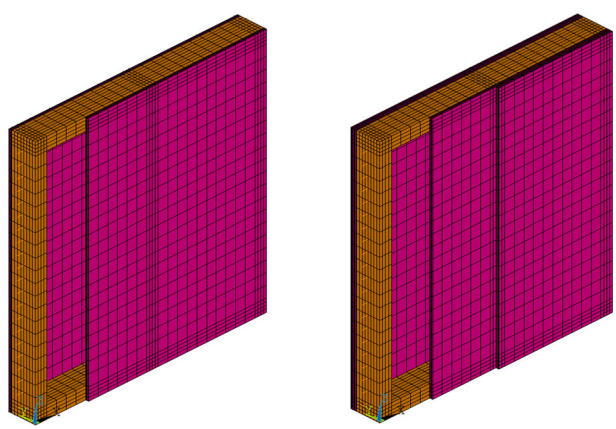

Fig. 6 Finite element mesh for both specimens

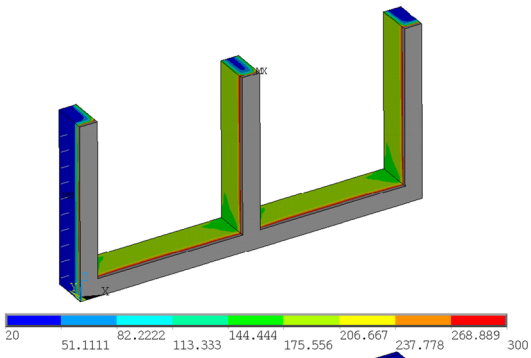

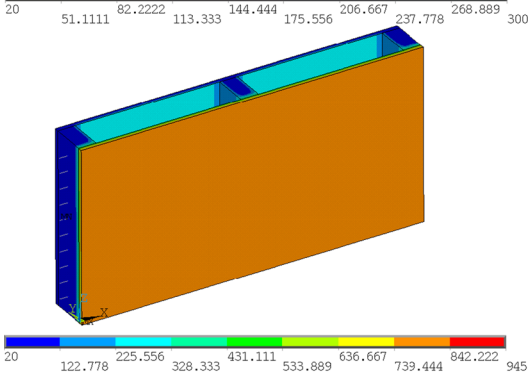

(a) Specimen 01 after 30 [min].

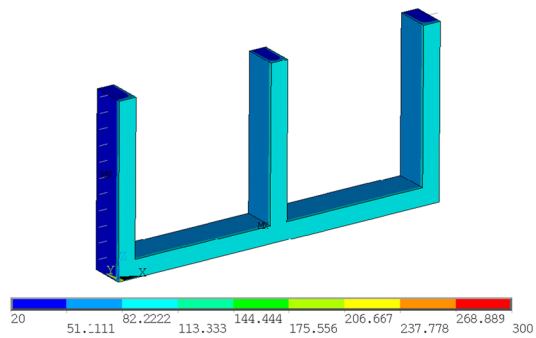

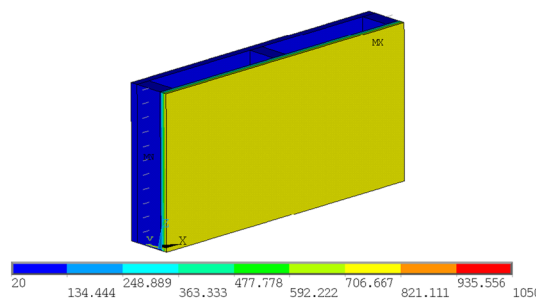

(b) Specimen 02 after 30 [min].

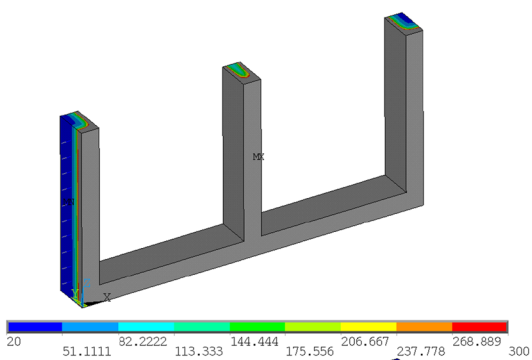

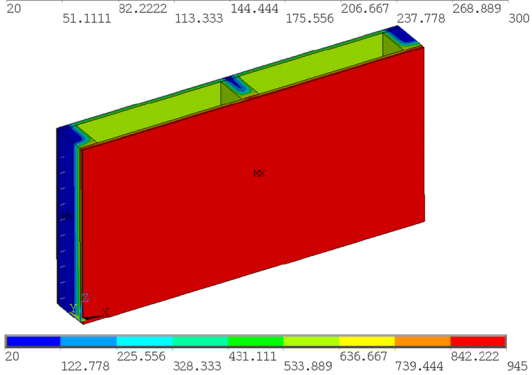

(c) Specimen 01 after 60 [min].

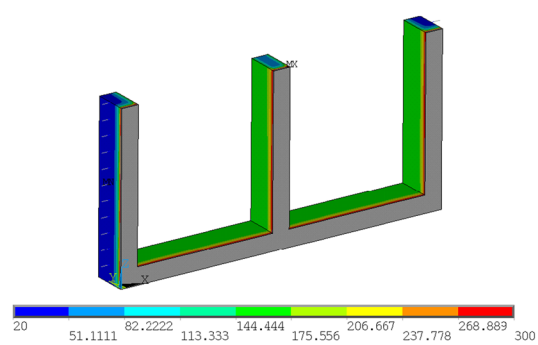

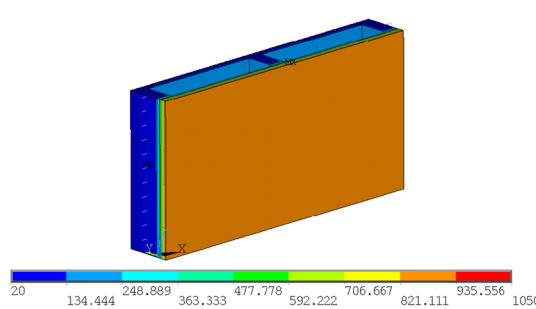

(d) Specimen 02 after 60 [min].

Fig. 7 Temperature results after 30 and 60 min of fire exposure

Table 9 Fire resistance for insulation

	T_{max} (min)	T_{ave} (min)	t_{ins} [25]
Specimen 01	44	46	53
Specimen 02	91	91	87

Results are evaluated for every time step. Figure 7 depicts the temperature field for both materials and the charred zone (grey) of the timber elements, after 30 and 60 (min) of fire exposure. Specimen 02 has higher fire protection, which reduces the temperature in both materials for the same time being considered.

The formation of the char layer may provide effective protection against the heat flux, especially in large cross sections, reducing the charring rate. This LTFW also includes gypsum layers for fire protection. The failure time of this protection t_f is assumed to be coincident with the time to start the charring formation t_{ch} on the narrow side of the stud. The temperature of the wood surface, at this time, will be submitted to a higher bulk temperature from the fire compartment, conducting to higher charring rate, until the char layer achieves 25 mm. After that period of time the charring rate decreases, according to the model of EN1995-1-2 [17]. The position of the char line can be predicted for any exposure time, using the model of EN1995-1-2. The current version method differs from the expected method in the future version. Both can be compared with the numerical results. Figure 8 depicts the charring rate for all the solution methods. The notional design charring depth is herein presented by $d_{\text{char},n}$, being defined in the direction perpendicular to the narrow side of the central stud. The time used to the start of charring t_{ch} was considered equal to the failure time of the cladding t_f (fall off the gypsum plates). According to the results, the charring rate of the numerical model changes with time, for specimen 02. The numerical results are closer to the future version method of the EN1995-1-2.

The average and the maximum temperature are also calculated in the unexposed surface to determine the fire resistance due to insulation. The criterion is based on the increase of 140 °C for the average temperature (Tave) or 180 (°C) for the maximum temperature (Tmax), above the initial average temperature ($\bar{T}_0 = 20$ °C). Both results are presented in Table 9 and are based on the temperature results of every node located at mid-high of the unexposed surface. Table 9 also presents the results determined by the separation function method. The relative difference between the fire resistance for insulation from specimen 01 is 20%, but for specimen 02 is just 4%.

2.5 Finite Element Model for Mechanical Analysis

For the mechanical analysis, the hexahedron SOLID185 is used. This element has eight nodes, each with three degrees of freedom (translations in each spatial direction UX, UY; UZ), uses linear interpolating functions and full Gauss integration $2 \times 2 \times 2$, with enhanced strain calculation. This model also includes an interface element COMBIN39, used to model the lateral restrain effect of the frame used in the furnace. According to the standard used for testing these elements, EN1365-1 [2], the width of the test specimen is less than the opening in the test frame, with a clearance between 25 and 50 (mm) from the lateral edges of the test specimen. This clearance only restrains the motion of the wall studs to the outside region, but should not offer any restrain in the opposite direction of the stud. This element behaves mainly under compression load, according to Fig. 9.

The load bearing is determined for this loading condition, but depends on the initial condition on the geometry and material (imperfections). Different deformed shape modes may be expected for the LTFW structure. A global imperfection, based on the maximum out of straightness equal to $H/300$ (H = height of the wall), is applied to the first instability mode to update the initial geometry. Using this initial geometry, the vertical load versus the contraction "C" of the structure has been determined at room temperature, see Fig. 10.

The solution method is incremental in displacement and iterative. The software uses the Newton Raphson method to determine the new equilibrium position for the structure when the displacement on the top is forced to compress the timber frame. The total reaction or load bearing (F) is determined on the top nodes, where the displacement is

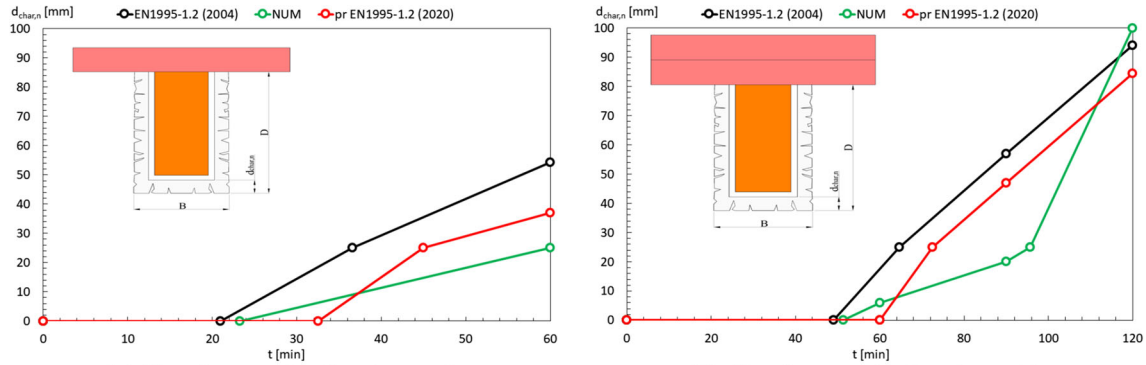

(a) Charring rate for Specimen 01 **(b)** Charring rate for Specimen 02

Fig. 8 Notional design charring depth

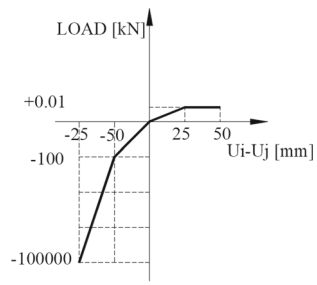

Fig. 9 Load–deflection curve for COMBIN39 finite element (not in true scale)

applied, for each equilibrium position. The incremental displacement is applied on the top of the LTFW structure, with a typical incremental displacement of 0.01 (mm), which can change between 0.001 and 1 (mm), depending on the convergence process. The criterion used to achieve the convergence is based on the internal forces, using a tolerance value of 5%. Here one can assume the existence of the external load $\{F\}$, which must be in equilibrium with the internal forces corresponding to the stress field $[\sigma]$. The final version of the equilibrium may be expressed, in every cartesian coordinate, according to Eq. 17.

The load bearing relation with respect to the vertical contraction has a variable shape. Starts with a linear branch, followed by a non-linear trend up to the maximum load, reached for $C = 12$ (mm). The instability changes the load bearing capacity, being the deformed shape mode of the central stud responsible for the timber frame failure. Equation (17) represents the static equilibrium to be determined for each fire rating time, considering the convergence for each load step, when applying the incremental load procedure.

$$\nabla [\sigma] + \{F\} = \{0\} \tag{17}$$

The fire resistance has been determined for certain fire rating times, using the temperature field corresponding to this rating time and the same incremental and iterative procedure to determine the load bearing capacity.

Figure 11 presents the reduction of the load bearing capacity for both specimens. The reduction has been determined based on the measurement of the load for the same vertical contraction ($C = 2.2$ [mm]), because different deformed shape modes are expected. These deformed shape modes depend on the charred layer of the timber frame and on the temperature field.

The temperature field is defined by the level of thermal protection given by the gypsum layers. Specimen 01 presents only one gypsum layer, which means that after 30 (min), the load bearing capacity of this specimen is smaller than the load bearing of specimen 02 (using two protection layers of gypsum).

The same specimen can achieve different deformed shape modes for the ultimate state, see Fig. 12, as an example for specimen 02, after 30, 60, 90 and 120 (min). The deformed shape mode for the central stud, after 120 (min), presents an out-of-plane displacement towards the fire exposed side. This mode shape is explained by the amount of charred layer, being the most unexposed fibre responsible to sustain the residual compressive load. The in-plane

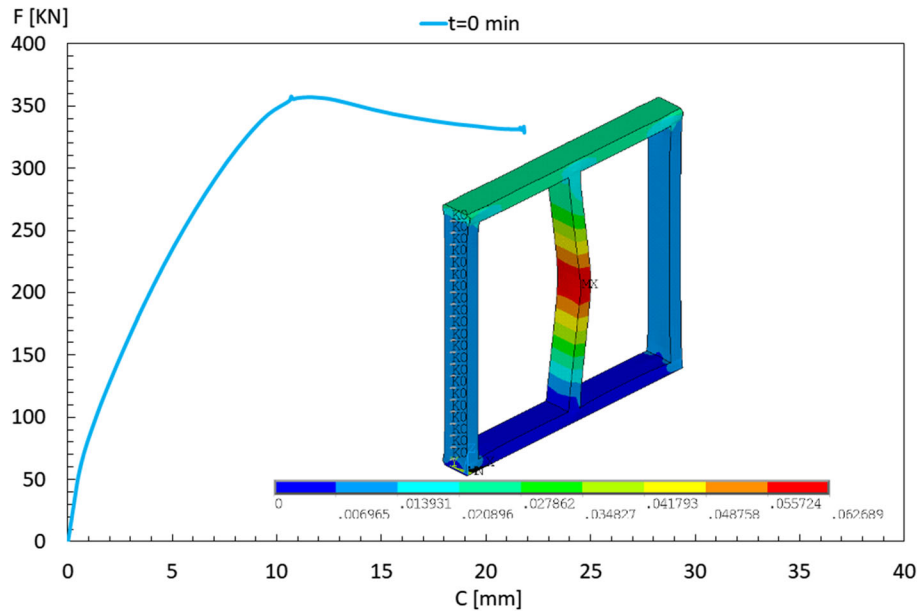

Fig. 10 Load bearing capacity of the LTFW at room temperature

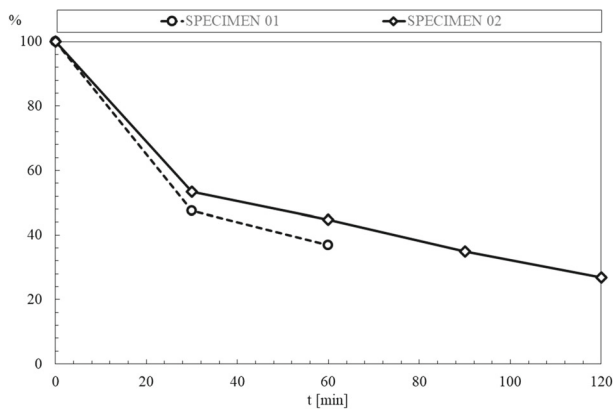

Fig. 11 Load bearing reduction of the LTFW under fire exposure

deformed mode shape may also be explained by the asymmetrical temperature field in the most external studs, due to the thermal protection of the specimen in the lateral edges, due to the contact with insulation material used for the clearance, see Fig. 7. The results for 90 (min) show an out-of-plane displacement towards the unexposed side, simultaneously with the in-plane buckling around the weak axis for the external studs of the frame. The results for 30 (min) present a flexural torsional buckling mode for the central stud. Similar behaviour is determined for 60 (min), but less pronounced for the central stud.

The same specimen can experience different deformed mode shapes, depending on the temperature field expected to the specified in fire rating and the amount of charred layer. Specimen 02 is found to have out-of-plane displacement of the central stud towards the unexposed side at 90 (min). The deformed shape mode depends on the temperature and char layer developed during the continuous development of the fire, which may explain these different deformed shape modes. The same specimen submitted to transient standard fire would first move towards the furnace side and several minutes later would go in the opposite direction. This is just to point out that, in these simulations, the temperature field is constant (steady) and can lead to a different deformed mode shape of the LTFW structure.

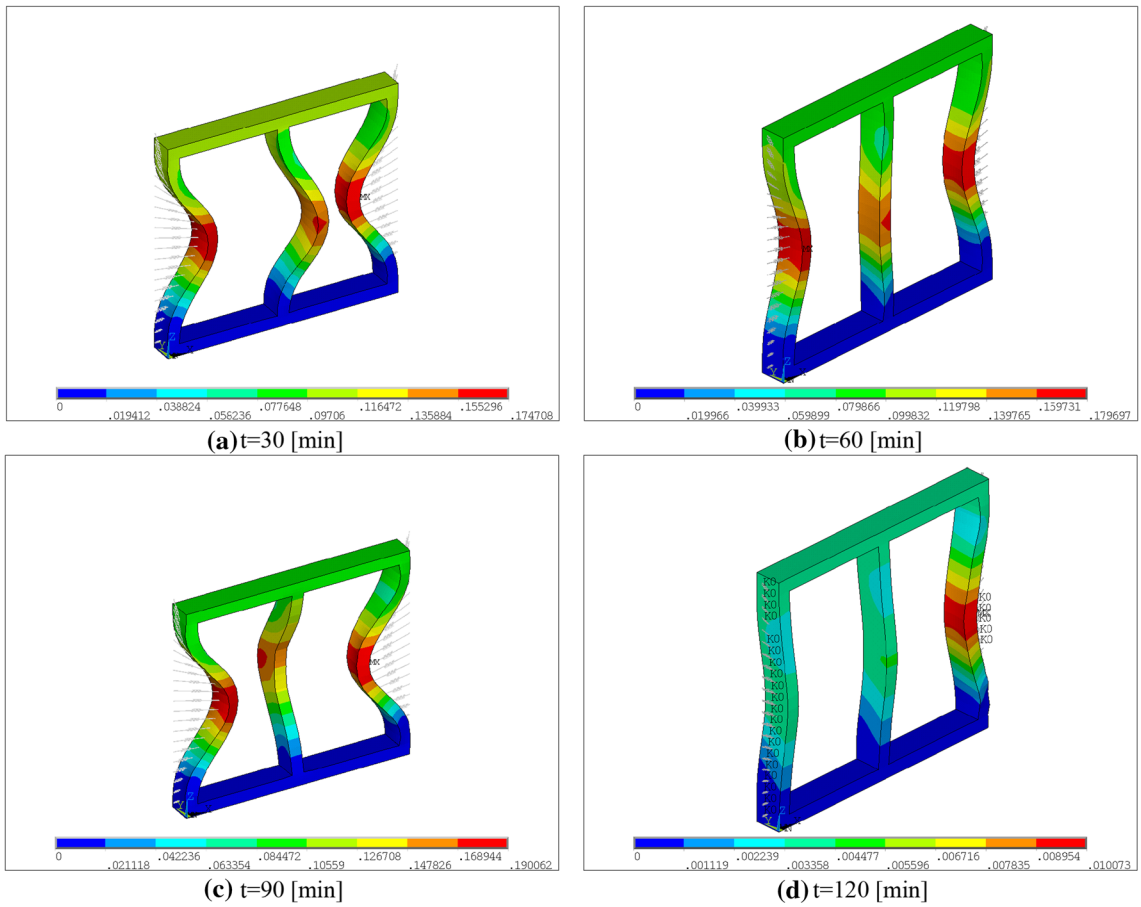

Fig. 12 Deformed shape modes for the LTFW after 30, 60, 90 and 120 (min)

3 Conclusions

This research presents the load bearing capacity of LTFW protected with one and two layers of gypsum at room temperature and after different fire rating periods. The finite element model for the thermal analysis has already been validated, which demonstrates the ability to predict accurately the temperature field in the timber frame.

Higher fire protection level reduces the charred layer of the studs for the same exposure time and increases the load bearing capacity. The load bearing reduces with the increase of fire exposure time, as expected. After 30 min, the load bearing is 53.5% for specimen 01 and 47.5% for specimen 02. This difference also increases after 60 min.

The charring depth has been determined for each of the specimens and compared with the prediction of the European charring model. The numerical results are closer to the method presented in the future version of Eurocode 5, part 1.2. According to the numerical results, and especially to specimen 02, different charring rates have been identified in the principal direction of the fire effect (wall thickness), changing between 0.7 and 3.8 (mm/min).

More simulations are expected to be developed based on different levels of protection layers, using different materials. Experimental tests are also still required to validate the load bearing capacity.

References

1. CEN, "EN 1363-1: Fire resistance tests Part 1: General Requirements." CEN- European Committee for Standardization, Brussels, p. 52 (2020)
2. CEN, EN 1365-1: Fire resistance tests for loadbearing elements-Part 1: Walls, CEN. Brussels: CEN (2013)
3. ISO, ISO834-1: Fire-resistance tests - Elements of building construction-Part 1: General requirements. International Organization for Standardization (1999)
4. CEN, EN 1364-1: Fire resistance tests for non-loadbearing elements. Part 1: Walls, CEN. Brussels: CEN (2015)
5. CEN, EN 13501-2: Fire classification of construction products and building elements-Part 2: Classification using data from fire resistance tests, excluding ventilation services, CEN. Brussels: CEN (2016)
6. Takeda, H., Mehaffey, J.R.: WALL2D: A model for predicting heat transfer through wood-stud walls exposed to fire. Fire Mater. **22**(4), 133–140 (1998). https://doi.org/10.1002/(SICI)1099-1018(1998070)22:4%3c133::AID-FAM642%3e3.0.CO;2-L
7. Piloto, P.A.G., Fonseca, E.M.M.: Timber framed walls lined with gypsum plates under fire. In: 7th International Conference Integrity-Reliability-Failure, pp. 547–556 (2020)
8. Gernay, T.: Modelling thermal performance of gypsum plasterboard-lined light timber frame walls using SAFIR and TASEF. Fire Mater. **34**(8), 385–406 (2010). https://doi.org/10.1002/fam.1026
9. Franssen, J.-M.: SAFIR. A thermal/ tructural program modelling structures under fire. Eng. J. Am. Inst. Steel Constr. **42**(3), 143–158 (2005). https://www.aisc.org/SAFIR-A-Thermal-and-Structural-Program-for-Modeling-Structures-Under-Fire
10. Sterner, E., Wickstrom, U.: TASEF—temperature analysis of structures exposed to fire-Users manual. Boras (1990). https://www.diva-portal.org/smash/get/diva2:961683/FULLTEXT01.pdf
11. Thi, V.D., Khelifa, M., Oudjene, M., El Ganaoui, M., Rogaume, Y.: Numerical simulation of fire integrity resistance of full-scale gypsum-faced cross-laminated timber wall. Int. J. Therm. Sci. **132**(June), 96–103 (2018). https://doi.org/10.1016/j.ijthermalsci.2018.06.003
12. Bedon, C., Fragiacomo, M.: Experimental and numerical analysis of in-plane compressed unprotected log-haus timber walls in fire conditions. Fire Saf. J. **107**(December 2017), 89–103 (2019). https://doi.org/10.1016/j.firesaf.2017.12.007
13. Fonseca, E.M.M., Leite, P.A.S., Silva, L.: Wood connections under fire conditions protected with gypsum plasterboard types A and F. In: Advances in Fire Safety Engineering, pp. 93–106 (2020)
14. Qin, R., Zhou, A., Chow, C.L., Lau, D.: Structural performance and charring of loaded wood under fire. Eng. Struct. **228**(2020), 111491 (2021). https://doi.org/10.1016/j.engstruct.2020.111491
15. Piloto, P., Khetata, M., Gavilán, A.: Fire resistance tests of non-loadbearing LSF walls. In: TEST&E 2019—2nd Conference on Testing and Experimentations in Civil Engineering—Proceedings, pp. 429–440 (2019). https://doi.org/10.5281/zenodo.3355354
16. Khetata, S.M., Piloto, P.A.G., Gavilán, A.B.R.: Fire resistance of composite non-load bearing light steel framing walls. J. Fire Sci. **38**(2), 136–155 (2020). https://doi.org/10.1177/0734904119900931
17. CEN, "EN 1995-1.2, Eurocode 5: Design of timber structures-Part 1–2: General-Structural fire design. CEN-European Committee for Standardization, Brussels, pp. 1–69 (2004)
18. CEN, "pr EN 1995-1.2, Eurocode 5: Design of timber structures—Part 1–2: General-Structural fire design." CEN-European Committee for Standardization, Brussels (2020)
19. Sultan, M.A.: A model for predicting heat transfer through noninsulated unloaded steel-stud gypsum board wall assemblies exposed to fire. Fire Technol. **32**(3), 239–259 (1996). https://doi.org/10.1007/BF01040217
20. Holmberg, S., Persson, K., Petersson, H.: Nonlinear mechanical behaviour and analysis of wood and fibre materials. Comput. Struct. **72**(4), 459–480 (1999). https://doi.org/10.1016/S0045-7949(98)00331-9
21. Milhan, T.H.: Numerical study on wooden beams subjected to high temperatures (in Portuguese). Instituto Politécnico de Bragança, MSc thesis (2020)
22. Guan, Z.W., Zhu, E.C.: Finite element modelling of anisotropic elasto-plastic timber composite beams with openings. Eng. Struct. **31**(2), 394–403 (2009). https://doi.org/10.1016/j.engstruct.2008.09.007
23. Rodney, H., Soc, R.: A theory of the yielding and plastic flow of anisotropic metals. Proc. R. Soc. Lond. Ser. A. Math. Phys. Sci. **193**(1033), 281–297 (1948). https://doi.org/10.1098/rspa.1948.0045
24. Schleifer, V.: Zum Verhalten von raumabschliessenden mehrschichtigen Holzbauteilen im Brandfall, ETH Library (2009)
25. Frangi, A., Schleifer, V., Fontana, M.: Design model for the verification of the separating function of light timber frame assemblies. Eng. Struct. **32**(4), 1184–1195 (2010). https://doi.org/10.1016/j.engstruct.2009.12.044
26. Nele Mäger, K., Just, A., Frangi, A., Brandon, D.: International network on timber engineering research. In: International Network on Timber Engineering Research, pp. 439–451 (2017)
27. Nele, M.K., Alar, J., Frangi, A.: Improvements to the component additive method. In: 10th International Conference on Structures in Fire, pp. 283–290 (2018)
28. CEN, "EN 1991-1-2, Eurocode 1: Actions on structures—Part 1–2: General actions—Actions on structures exposed to fire," CEN-European Committee for Standardization. CEN- European Committee for Standardization, Brussels, p. 59 (2002)
29. Dai, B., Zheng, B., Liang, Q., Wang, L.: Numerical solution of transient heat conduction problems using improved meshless local Petrov–Galerkin method. Appl. Math. Comput. **219**(19), 10044–10052 (2013). https://doi.org/10.1016/j.amc.2013.04.024